Project: “Monitoring Sea-water intrusion in coastal aquifers and Testing pilot projects for its mitigation” Interreg CBC Italy-Croatia 2014.-2020.

Priority Axis: Safety and resilience

Specific objective: Improve the climate change monitoring and planning of adaptation measures tackling specific effects, in the cooperation area

(D_4.1.1) Input for the characterization and the numerical model: 3D hydro-geophysical setting of the Neretva plain in dry/salt and wet/fresh hydrologic conditions initial report on wet/dry season conditions

Work Package 4: Testing

Activity 1: Neretva coastal plain

Partner in charge: PP4 (UNIST-FGAG)

Partners involved: PP4 (UNIST-FGAG), PP5 (CROATIAN WATERS), PP6 (DUNEA)

Final version

Public report

September, 2022

1 Contents

2 Introduction

This report is composed on the basis of data delivered acquired by GeoTechnologies LLC, processed and inverted by EMergo. The data is from an EQUATOR airborne geophysical survey carried out in Neretva, Croatia, between 26th-28th October 2021. The location map of the AEM data, effectively considered for the inversion after deleting of noisy data (affected by infrastructures) is shown in Figure 2.1 (black dots). The final goal of the AEM project is to improve and update the understanding of the groundwater resources in the area.

Attached to the present report there are two databases containing respectively the data used for the inversion, and the inversion results.

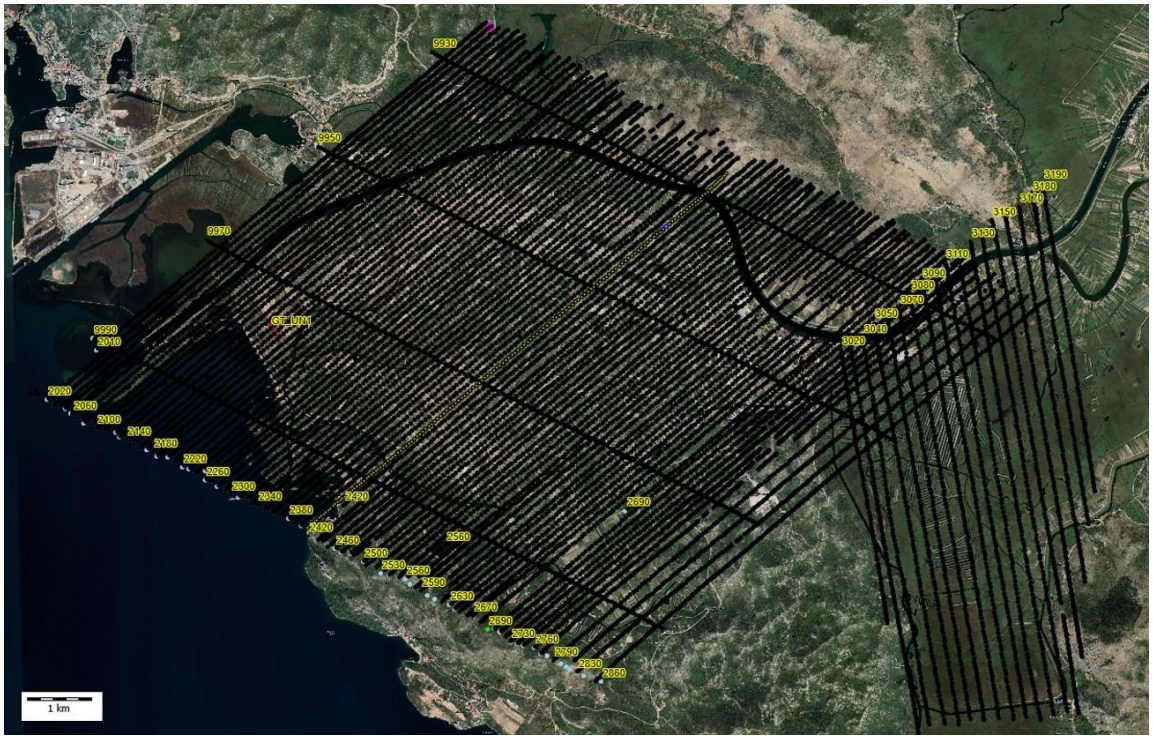

Figure 2.1. Location map of the survey area. The sounding locations are represented by the blackdots.

3 The EQUATOR system

EQUATOR is a time-domain helicopter electromagnetic system designed for hydrogeophysical, environmental, and mineral investigations. The system is shown in operation in Figure 2. The EQUATOR system is carried as an external sling load powered by the helicopter. The transmitter, mounted on a lightweight fiberglass frame, consists of 4 turns of 4 m radius. The maximum peak of the current flowing in the transmitter is 550 A. The three-component receiver is placed 27 m above and 30 m ahead of the transmitter frame. Radar altimeters are on the frame measuring continuously the distance to terrain while the system is designed to be inherently horizontal no matter what the helicopter velocity is.

Measurements are carried out continuously while flying. Every single transient is stored in a binary format, and pre-stacked. The 14 off-time channels range from 5 µs to 4.5 ms (center times) from the end of the ramp.

Together with altitude and EM data, a number of instrument parameters are monitored and stored digitally so that they can be used for quality control when processing the data.

The EQUATOR system measures also on-time data, which can eventually be exploited when the observations are returned in frequency-domain (from 77 Hz to 16 000 Hz – X, Y, Z-components).

In this preliminary phase of the project, only the time-domain data have been used and will be discussed in the present report.

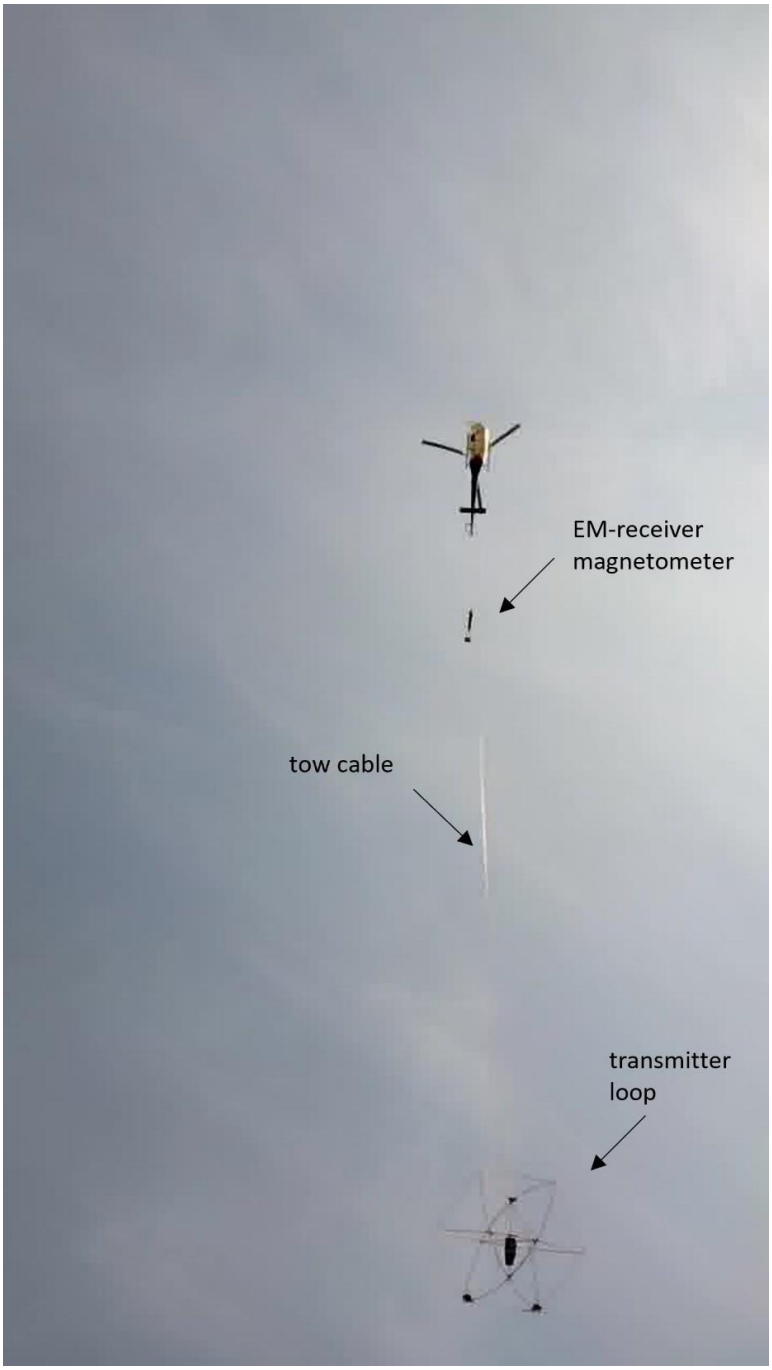

Figure 3.1 The EQUATOR system

4 Data collection

The time-domain data are collected always on-time as it is clear from the used waveform depicted in Figure 4.1. The period of the waveform (including both the positive and negative half-period) is typically 13 ms (corresponding to a base frequency of 77Hz). The associate frequency spectrum of the signal is shown in Figure 4.2.

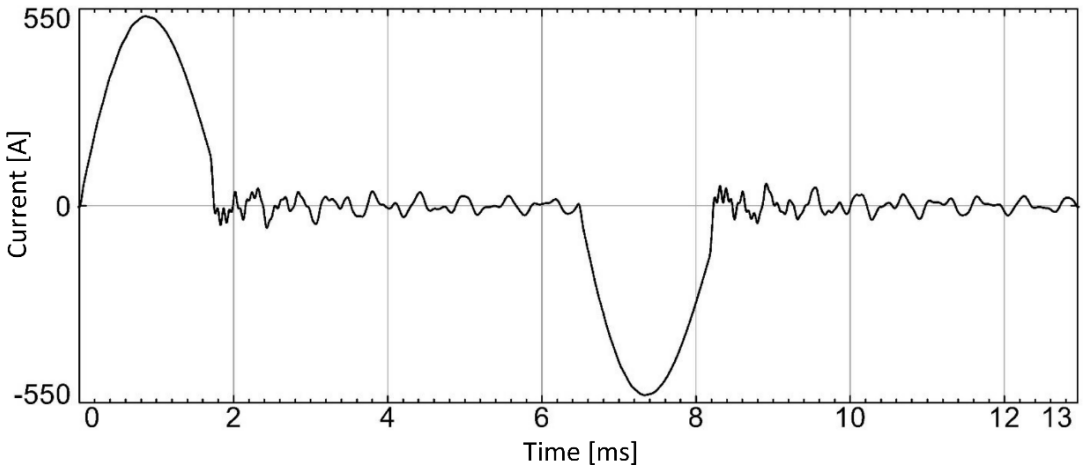

Figure 4.1 The EQUATOR system waveform

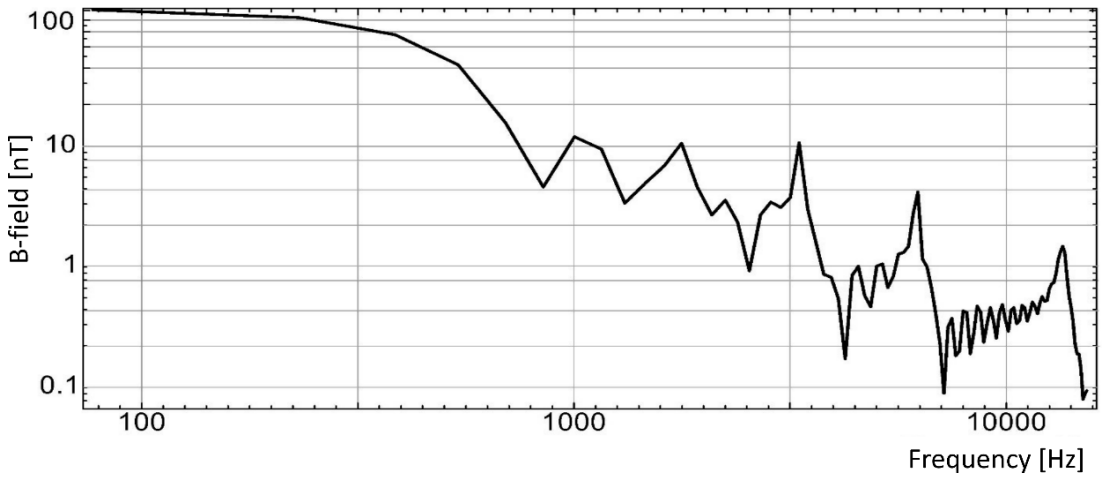

Figure 4.2 The EQUATOR system frequency spectrum

The responses (sampled at 200 kHz) are returned in the frequency-domain in the corresponding in-phase and quadrature components for each of the odd harmonics between 77.16 Hz and 15355 Hz and then stacked into 14 frequencies: 77 Hz, 231 Hz, 385 Hz, 540 Hz, 694 Hz, 1003 Hz, 1157

Hz, 1311 Hz, 1466 Hz, 1620 Hz, 1775 Hz, 3163 Hz, 6250 Hz, 13503 Hz. In this respect, the apparent resistivities derived from the measurements at selected frequencies are plotted in Figure 4.3Figure 4.6. It should be highlighted that, in general, the apparent resistivities maps cannot be considered to be representative of the true resistivities; the associated possible ambiguities are in any case solved during the inversion phases.

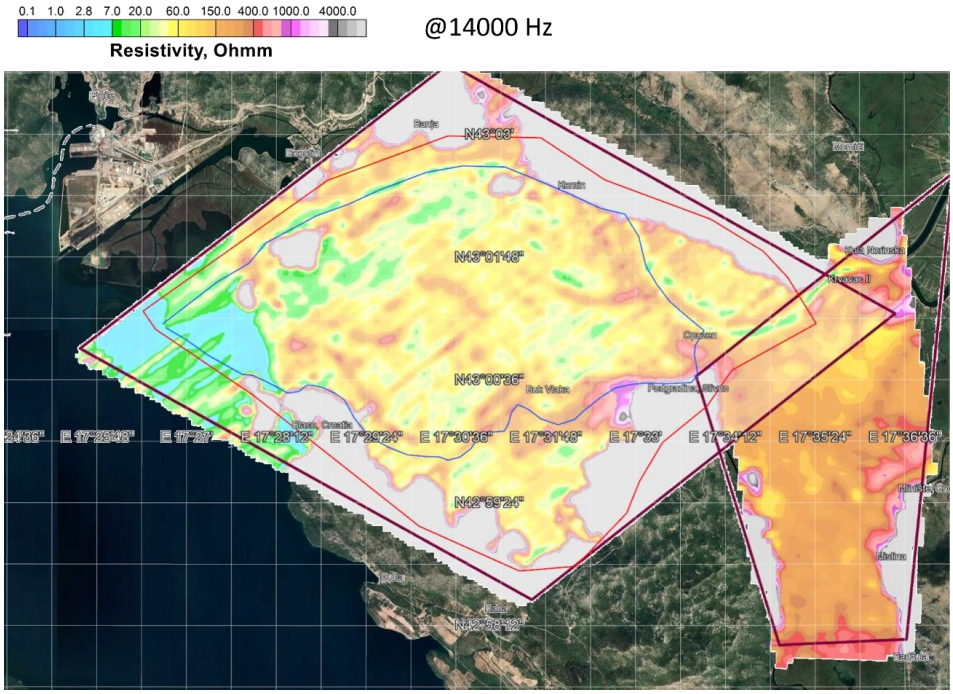

Figure 4.3 The apparent resistivity map derived by the measurement at 14 kHz. The thin red line delimits the target area; the thick dark-red polygons delimit the survey areas; the blue thin lines show the paths of the Neretva River (in the north), and the Mala Neretva branch (in the south).

The frequency-domain data can be inverted as they are after a few processing steps, further increasing the robustness of the data. By retaining all the original information content of the original observations, the frequency-domain data inversion is in principle capable to retrieve more details about the shallow subsurface. And, as will be elaborated later while discussing the results,

already the spatial coherence of the apparent resistivity maps derived by the frequency-domain measurements could provide useful insights about the target area.

However, since, at these preliminary stages, the priority is to assess the information content at depth, mainly in the attempt to map the bedrock, the data have been processed and inverted in the time-domain. In fact, the frequency-domain data is translated time-domain (off-time) data and is provided by Geotechnologies LLC as 14 time-gates ranging from 2.5 µs to around 3.5 ms as shown in Figure 4.12. In time-domain, the data have been inverted by the state-of-the-art tools byEMergo.

The maps of the dB/dt measurements for the first 12 time-gates generally used for the inversions are shown in the Figure 4.7Figure 4.18. The not-perfect leveling of the dB/dt values for the late time-gates between different flights is limited and it should not significantly affect the inversion results. In any case, in future processing and inversion iterations, it will be easily solved.

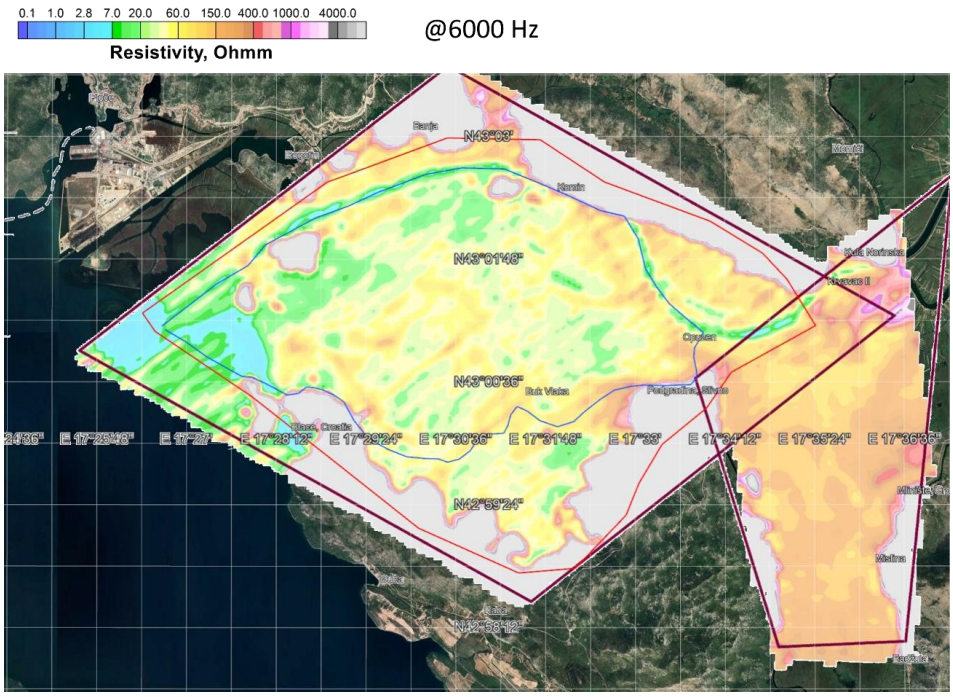

Figure 4.4 The apparent resistivity map derived by the measurement at 6 kHz.

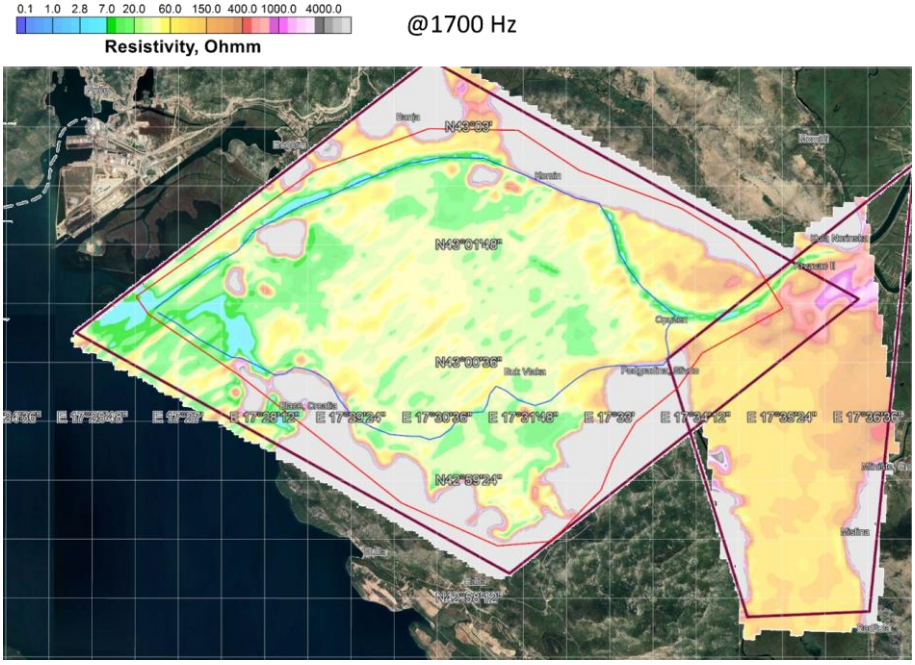

Figure 4.5 The apparent resistivity map derived by the measurement at 1.7 kHz

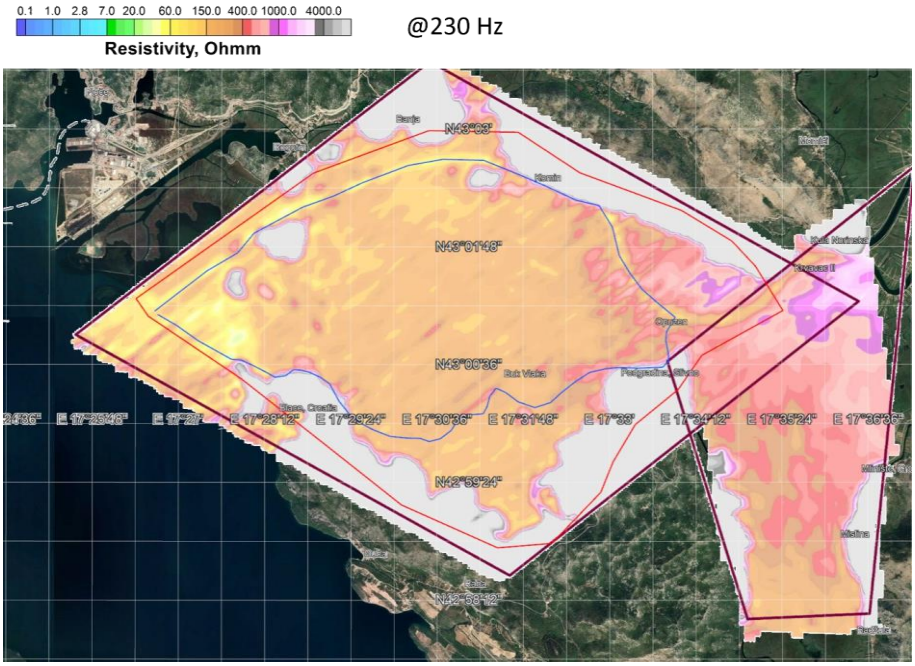

Figure 4.6 The apparent resistivity map derived by the measurement at 0.230 kHz.

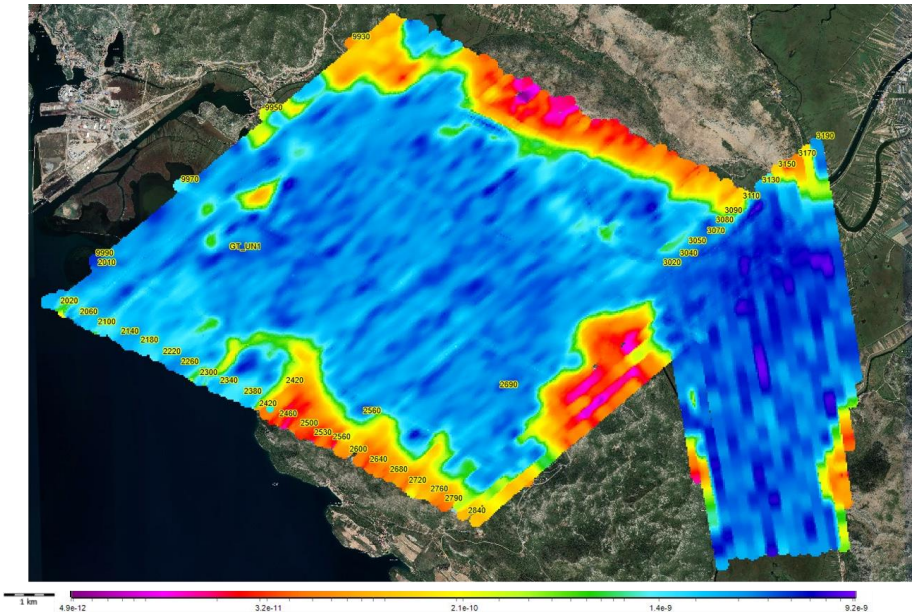

Figure 4.7 The dB/dt (Z-component) map at the 1st time-gate (2.5 μs)

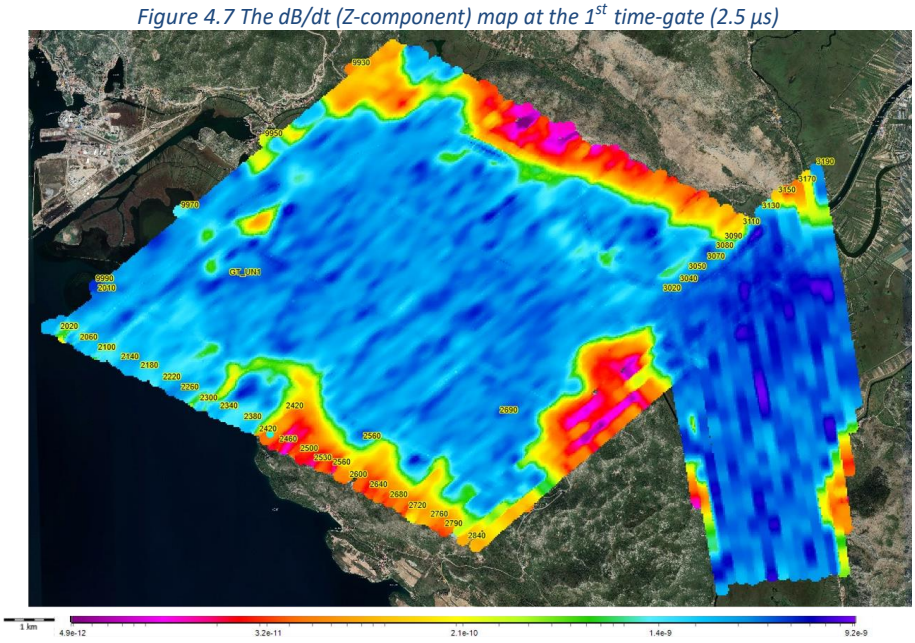

Figure 4.8 The dB/dt (Z-component) map at the 2nd time-gate (7.5 μs).

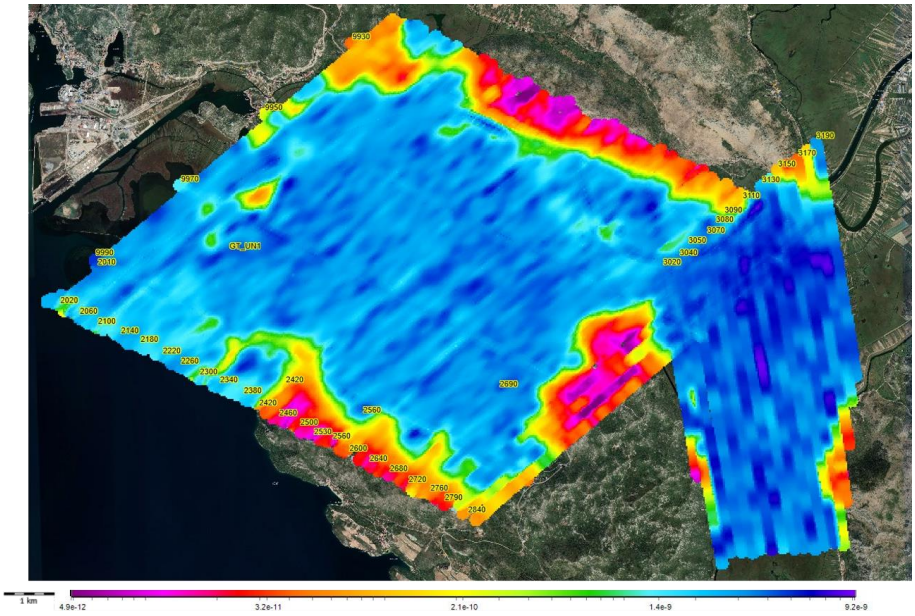

Figure 4.9 The dB/dt (Z-component) map at the 3rd time-gate (15 µs).

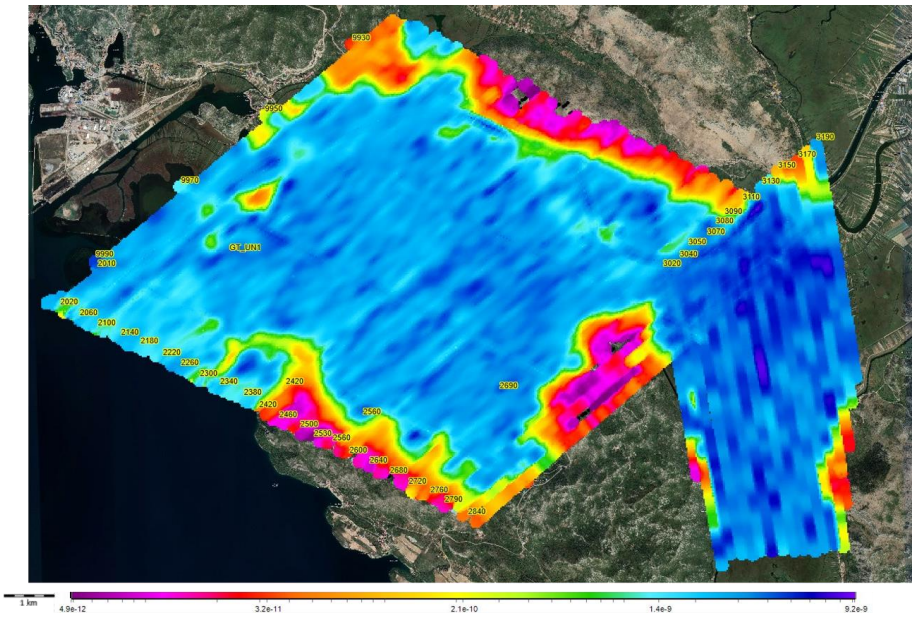

Figure 4.10 The dB/dt (Z-component) map at the 4th time-gate (25 µs).

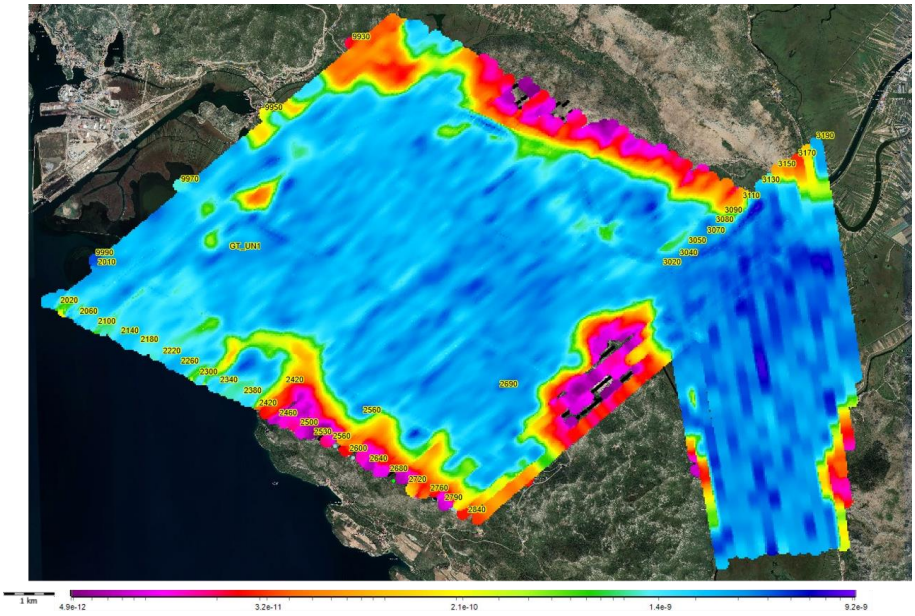

Figure 4.11 The dB/dt (Z-component) map at the 5th time-gate (42.5 μs).

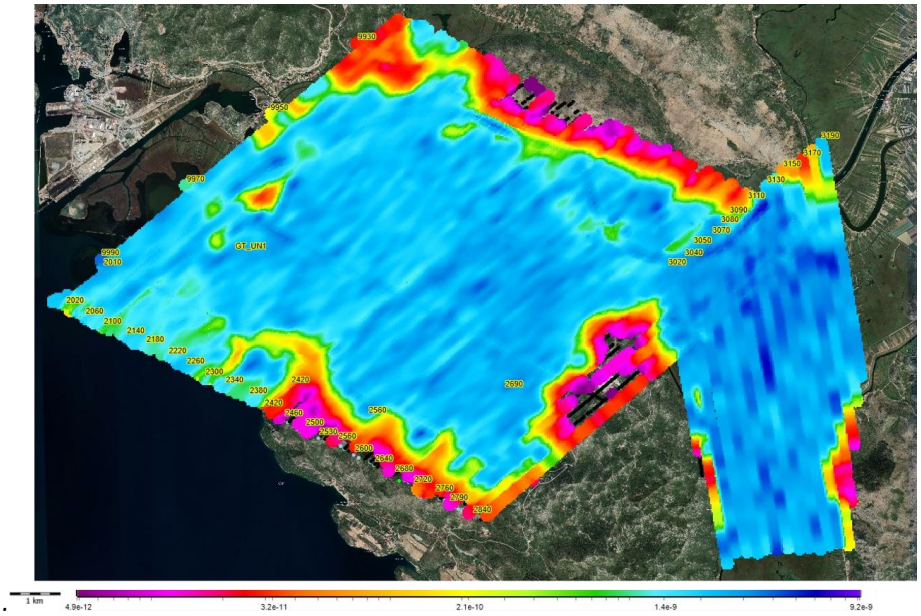

Figure 4.12 The dB/dt (Z-component) map at the 6th time-gate (72.5 μs).

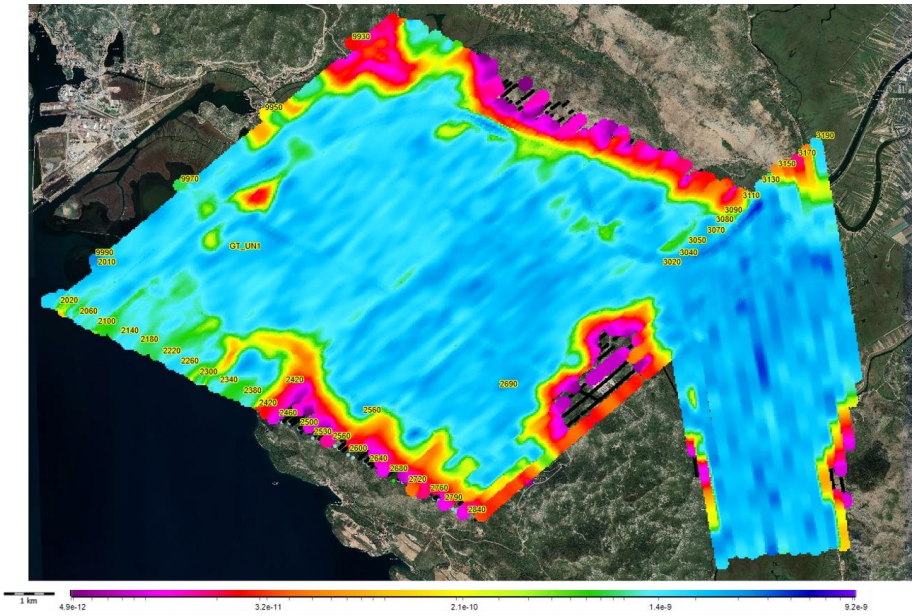

Figure 4.13 The dB/dt (Z-component) map at the 7th time-gate (117.5 µs).

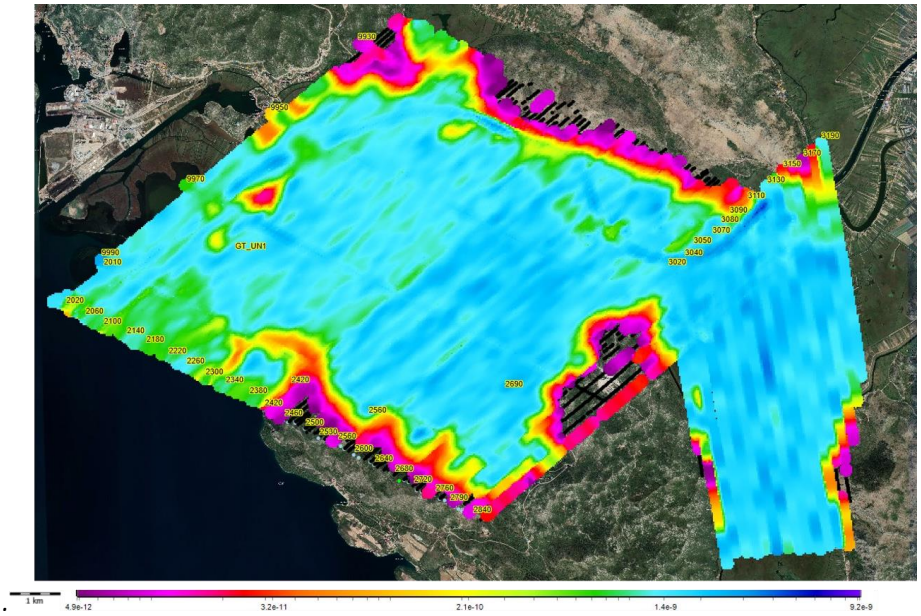

Figure 4.14 The dB/dt (Z-component) map at the 8th time-gate (192.5 µs).

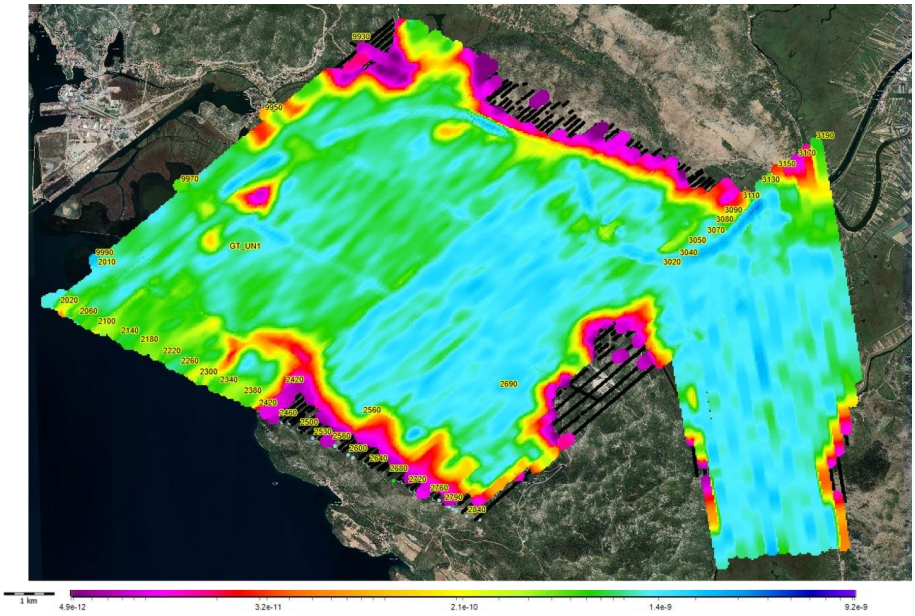

Figure 4.15 The dB/dt (Z-component) map at the 9th time-gate (315 µs).

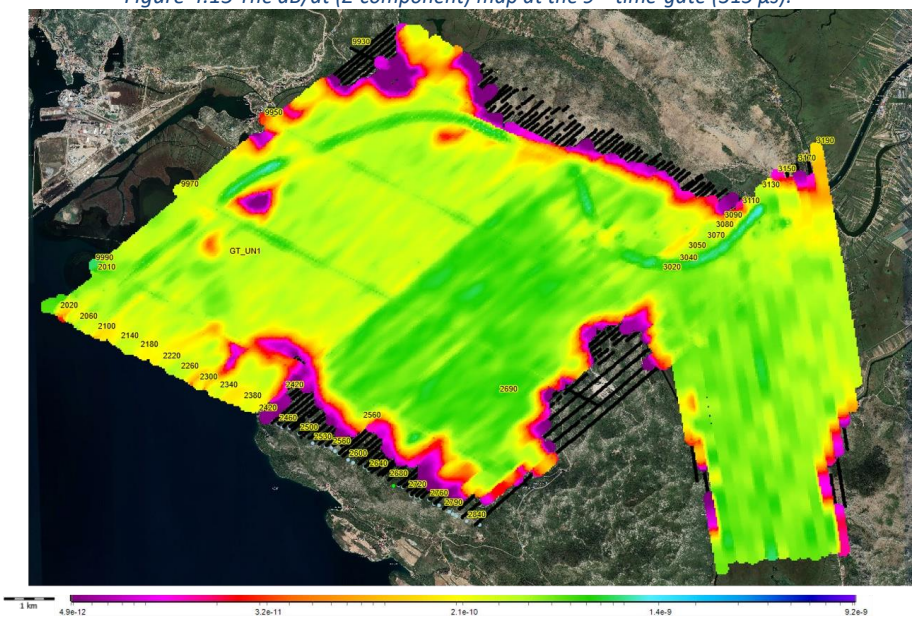

Figure 4.16 The dB/dt (Z-component) map at the 10th time-gate (512.5 µs).

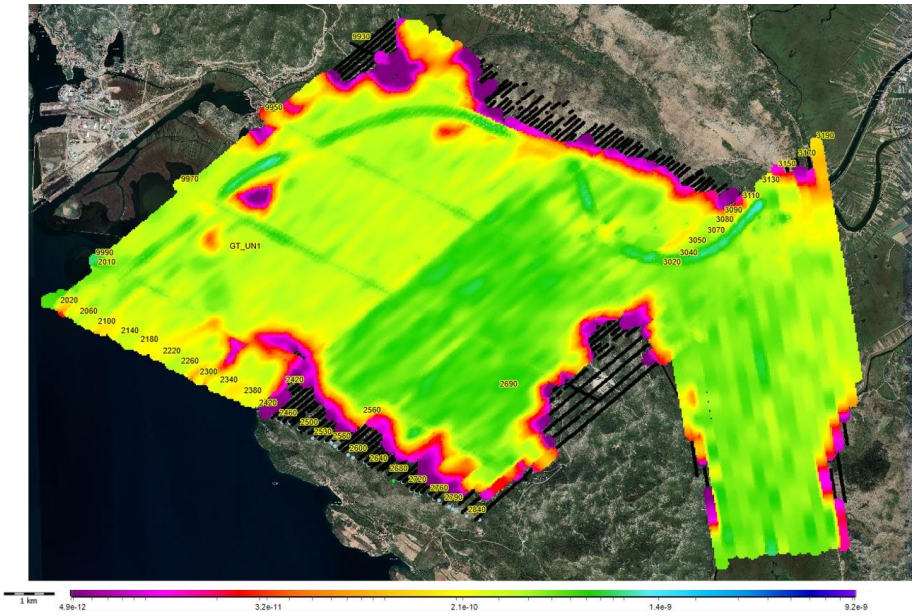

Figure 4.17 The dB/dt (Z-component) map at the 11th time-gate (832.5 μs).

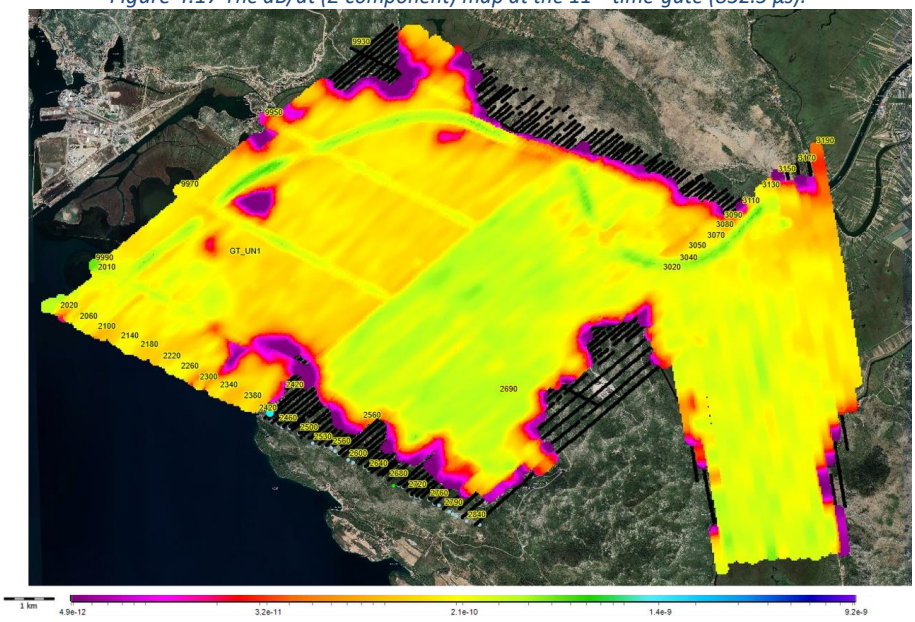

Figure 4.18 The dB/dt (Z-component) map at the 12th time-gate (1352.5 μs).

5 Processing

The aim of processing is to prepare data for the data inversion. This includes data import, data corrections, filtering, culling of distorted or noise-filled data. The data left are then averaged spatially using trapezoid filters designed with the optimal width to enhance the signal-to-noise level without significant reduction of the lateral resolution. Figure 5.1 shows the schematic workflow of the processing and inversion process.

All data are marked with a timestamp which is the key to binding information about current, altitude, GPS coordinates, etc. During the processing a running mean is calculated separately for the X- and Y direction tilt data while algorithms are used to automatically filter out bad altitude data - typically (at least in the case of laser altimeter) reflections from tree or bush tops.

In this survey, the first usable time gate used is around 2.5 µs after transmitter ramp-off.

The processing of voltage data is done in a two-step system: an automatic and a manual. In the former, the navigation data is corrected for e.g., the transmitter/receiver tilt, and altimeters drop, while for the EM data are deployed a number of filters designed to cull coupled or noise influenced data. Note: in order to preserve the integrity of the measured data, the processing is done on the raw, binary data rather than on the pre-filtered ASCII data.

After that, automatically processed raw soundings are inspected visually using a number of different data plots. At this stage, it is accessed whether the filters have removed the right amount of data coupled to man-made infrastructures. It is usually necessary to intervene manually to fine-tune the outcome of the filters and obtain the most reliable results. Figure 5.2 shows a view of the data over a section of the EQUATOR data (35 seconds).

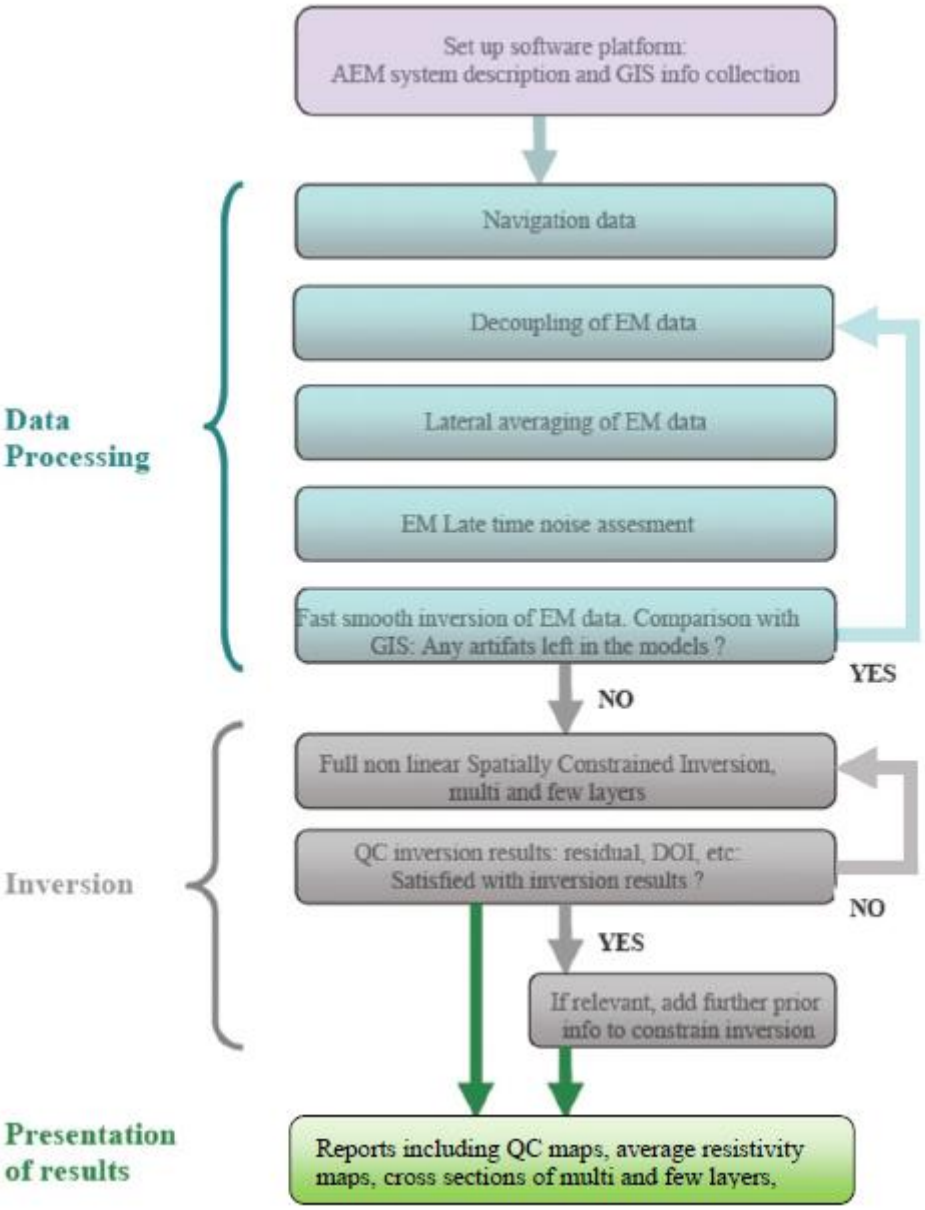

Figure 5.1 Workflow of the data processing and inversion of the EQUATOR data carried out byEMergo.

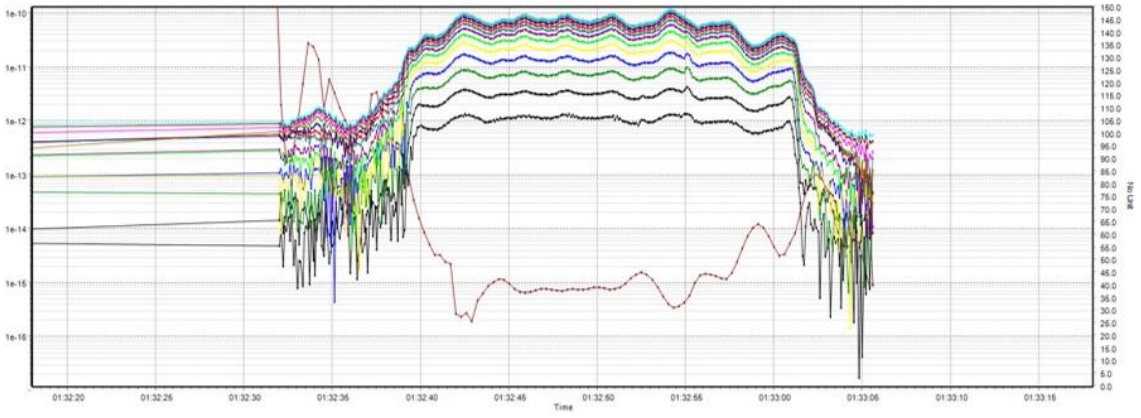

Figure 5.2 The data processing window. The brown solid line shows the altitude of the system,to be read on the right vertical axis.

In general, also the altimeter data need to be filtered (Figure 5.3). The aim of altimeter filtering is to remove laser or, in the specific case of the EQUATOR system, radar reflections that are not coming from the ground. This is done with an algorithm that takes advantage of the fact that spurious reflections, not generated from the soil surface, result in an apparent lower flight altitude than the remaining reflections. The algorithm filters out the data by repeatedly making a polynomial fit to the data and then removing data some meters below the latest polynomial fit. This automatic filtering is followed by a manual inspection and in some cases manual refinements. This is mostly needed in areas with problematic ground reflections. In such areas, it can be advantageous to calculate another flight altitude based on the above sea level altitude from the GPS and a digital elevation model. While less accurate than the flight altitude based on the radar reflections from the ground, this flight altitude can be used to guide the manual refinements.

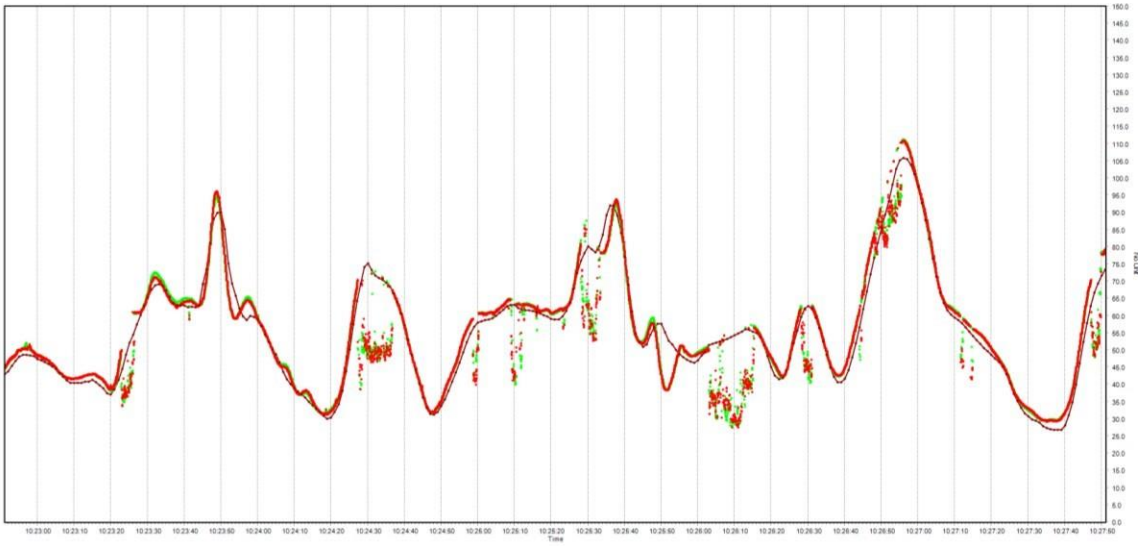

Figure 5.3 shows an example of processing of laser altimeter data.

EM data are then averaged to increase the signal-to-noise ratio data using a trapezoid-shaped averaging core, where the averaging width of late time data is larger than that of early time data, as seen in Figure 5.4.

The data uncertainty for these stacked (averaged) soundings is calculated from the data stack. Furthermore, a minimum level of uniform data uncertainty is assigned to all data. This uncertainty has been set to 3%.

Soundings were produced for every 1.0 s, corresponding to approximately 30 m. Table 5.1 providesa summary of the automatic filters applied to the dataset.

Figure 4.5 shows the effect of the filtering on the same data shown in Figure 4.2. The late time-gatesare often discarded (in grey), as they are below or close to the background noise.

After the automatic stacking, soundings are inspected visually using a number of different data plots. At this stage, it is assessed whether data points at late times should be ascribed a higher uncertainty or removed entirely. It is custom to cull data when the background noise level reaches the level of the earth response. Assessing when data is unusable is done by looking at the decay curves, the distance to potential noise sources, and the level of the background noise.

This process is necessary to obtain reliable model parameters in all parts of the data sections. Figure 5.6 shows two stacked soundings with different time gates displaying different noise levels (shown as vertical bars).

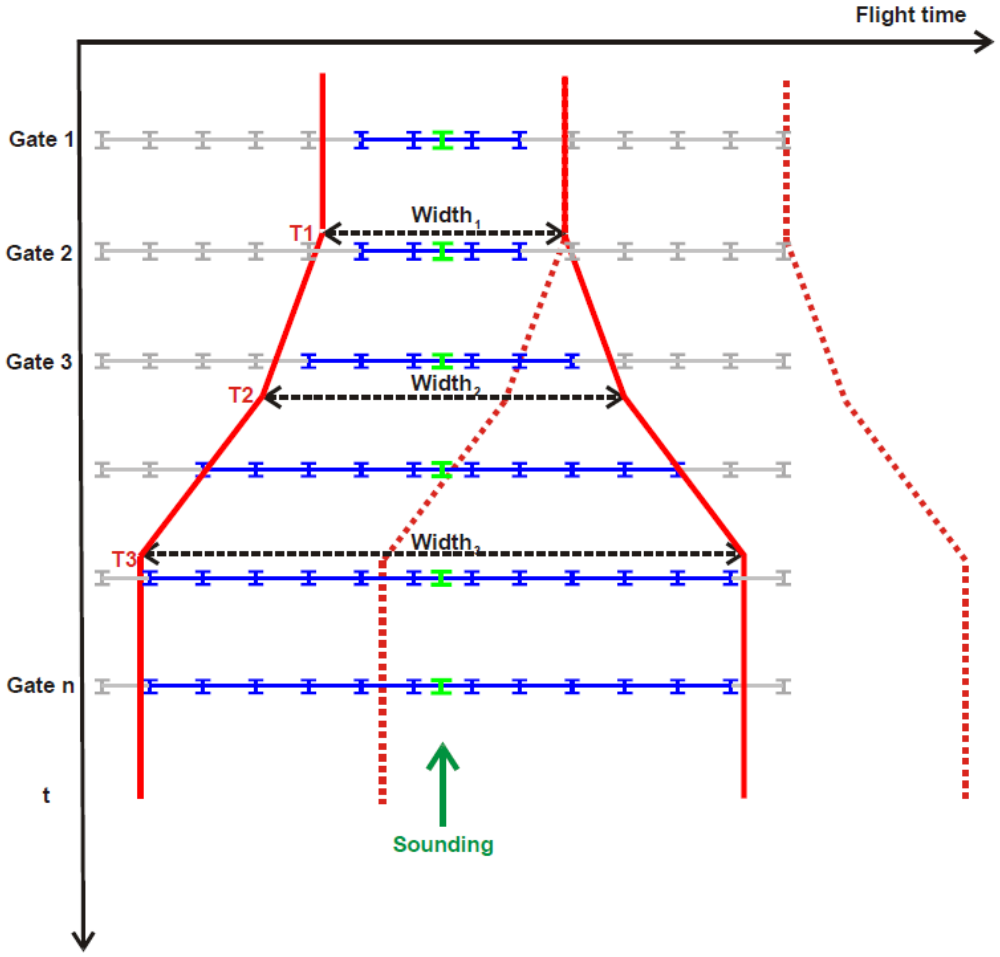

Figure 5.4 The rationale behind the trapezoidal averaging window is that lateral stacking overlarger time spans at later times increases the signal-to-noise ratio where, accordingly to thephysics of the method, the resolution is lower (late time-gates – larger depth), while keeping as much lateral resolution as possible at the early times where the footprint of the signal is smaller.

Table 5.1 The settings for the automated filters used in the first phase (automatic filtering) of theprocessing. All the data are expressed in seconds.

Distance between averaged soundings (s)	1
Time of first trapezoid knee point (T1)	1e-5
Time of second trapezoid knee point (T2)	1e-4
Time of third trapezoid knee point (T3)	3e-4
Width of first trapezoid section (width 1)	0.5
Width of second trapezoid section (width 2)	0.9
Width of third trapezoid section (width 3)	1.3

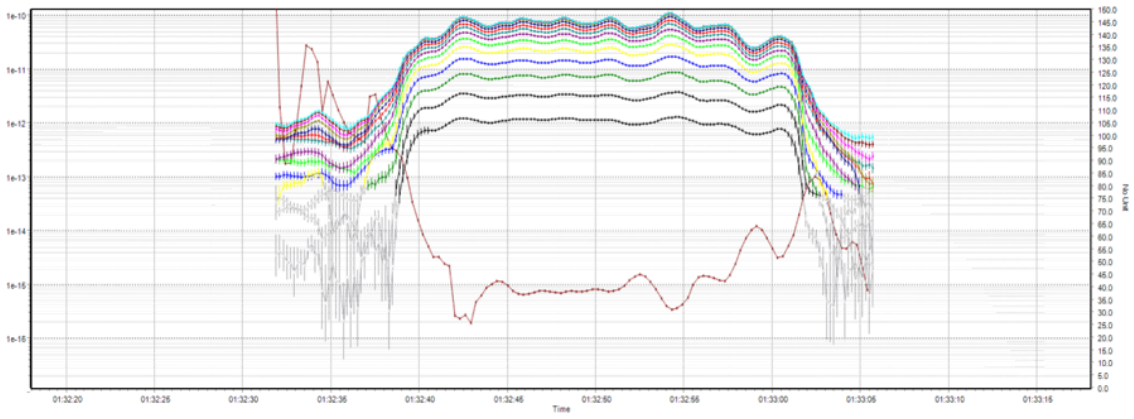

Figure 5.5 The data in Figure 5.3 after being laterally staked via the trapezoidal filter in Table 1.The grey data points are those removed as considered too noisy.

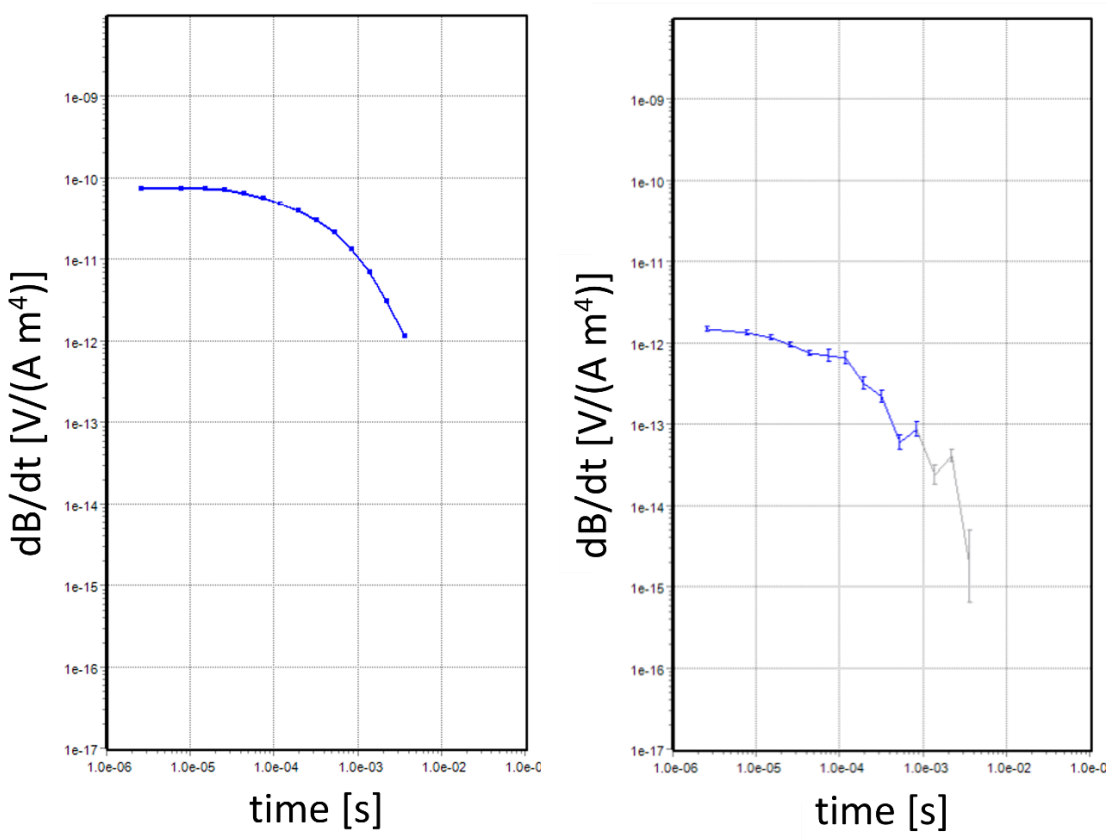

Figure 5.6 Example of averaged sounding with the different time-gates characterized bydifferent noise levels.Inversion

Preliminary inversions are carried out using the (quasi-)2-D Laterally Constrained Inversion (LCI). Final inversions will be carried out using the (quasi-)3-D Spatially Constrained Inversion (SCI). LCI and SCI are full non-linear damped least-squares solutions in which the transfer function of the instrumentation is modeled. This includes, among the others, current turn-on and -off ramps,and front-gate, system altitude. The inversion kernel is AarhusInv. This code allows running efficiently large inversions and was crucial in inversion testing and assessing in detail the model space.

Preliminary LCIs serve the purpose of fine-tuning the post-processing of the EM data, in terms of both couplings and noise assessment.

In the SCI scheme, the model parameters are tied together spatially with a spatially dependent model covariance which is scaled according to the distance between neighboring models.

Constraining the parameters tends to enhance the spatial coherence of the retrieved resistivity distribution and of the layer interfaces which might not be well resolved in an independent inversion of the soundings. The flight altitude is included as an inversion parameter with a prior value calculated from the radar altitudes. The standard deviation on this parameter is set to 1 m.

The LCI/SCI inversion scheme is developed for a parameterization of, in this specific case, 24 layers each having a fixed thickness, but a free resistivity. Traditionally, regularization (incorporating our a priori knowledge or assumptions) consists of a vertical smoothing constraints term (smooth inversion) applied to stabilize the inversion, e.g., to remove fictitious layers, especially in models based on few data points. Table 5.2 summarizes the main settings of the final smooth LCI, which, due to its flexibility, represents the current main output. The range of depths is from 4 to 400 m (at which an infinite half-space starts).

Table 5.2 LCI/SCI settings

Resistivity starting model (ohm-m)	From 10 to 200 Ohmm
Vertical Constraints	2
Lateral Constraints	3
Reference distance (m)	30
Power law distance drop off	0.75

The depth of investigation (DOI), based on an analysis of the Jacobian matrix, was also estimated for the output models. This DOI, is presented in a dedicated horizontal map, as well as superimposed to crop the average resistivity horizontal maps, and as a fading of colors below the DOI on the vertical cross sections. The DOI represents the maximum depth below surface to which there is sensitivity to the model parameters. It bears a degree of subjectivity in the selection of the threshold used to derive it (cfr.: Christiansen and Auken, 2012; Vignoli et al., 2021). As such, it is be treated as indicative. Any model parameter resting much below the DOI should however be considered highly uncertain as almost independent from the observations.

A further possibility of different regularization is a rather novel algorithm (Vignoli et al. 2015) based on an extension of the LCI/SCI (e.g., Auken and Christiansen 2004, Viezzoli et al. 2008). In this new algorithm, the regularization is not defined anymore as the L2 norm of the gradient of the solution, but as its gradient support. This approach is called sharp SCI (sSCI). So, insteadof searching for the model compatible with the observed data and with the minimum spatial variation of the solution (like the standard SCI), the sSCI regularization looks for the minimum number of spatial (vertical and/or lateral) variations, whilst fitting the data. It has the potential advantage of producing robust output models with sharper boundaries, more readily useful for subsequent geological modelling and data integration. The sSCI produces complementary results to the standard SCI and should be taken into account when performing any further geological/hydrogeological modelling of the results. However, in the present project, no sSCI inversion has been fully performed yet. So, in the present version of the report, only the more standard LCI results will be shown and discussed.

Additionally, we are planning to test the utility of applying a priori information in improving the resistivity modelling. For this goal, we might use the main lithological contacts drawn from the existing wells' stratigraphies, assuming they could be associated to reliable resistivity contrasts. This information might be fed into the inversion as extra data, with its associated degree of uncertainty.

6 Results

The results presented in this section are uniquely geophysical. Thus, the models show results obtained without the use of ancillary information as a priori to the inversion.

The inversion results are presented first as a series of Quality Control maps. The data fitting is generally acceptable: the map of misfit (Figure 6.1) shows values often lower than 0.6, hence 1D resistivity models are consistent with the measured data. The only part of the survey with a data misfit consistently higher than 1.5 is the offshore portion.

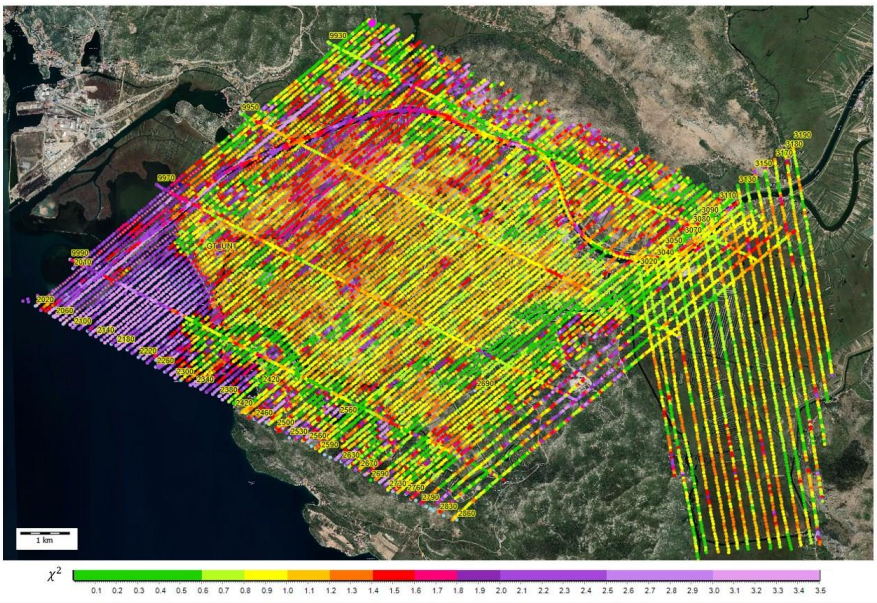

Figure 6.1 Data misfit for the smooth inversion.

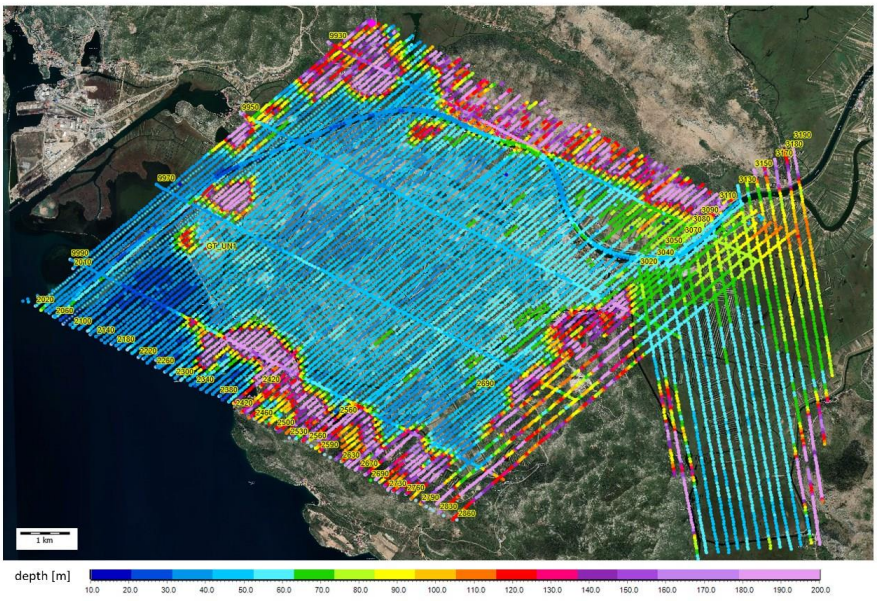

Figure 6.2 Depth of Investigation (smooth inversion, m b.g.l.).

Figure 6.2 shows the DOI for the smooth inversion. According to this estimate, the survey achieved reliable information to significant depths, almost everywhere down to 50-60 m. The lowest values (< 10 m) occur off-shore where the high conductivity of the seawater prevents to reach significant depth. For the same reason, on the borders of the survey area, in correspondence to the highs characterized by higher resistivity values, the DOI can reach larger depths.

The results of smooth modeling are represented both as horizontal and vertical slices. The first report a 2D interpolation (kriging) of the models, while the latter the individual 1D models projected along some of the flight lines.

The maps of average resistivity at different horizontal intervals (based on smooth inversion) are given in elevation above mean sea level, in Figure 6.3 – 6.6. All models are masked by DOI. Furthermore, some representative vertical resistivity sections are shown in Figure 6.7 -6.9.

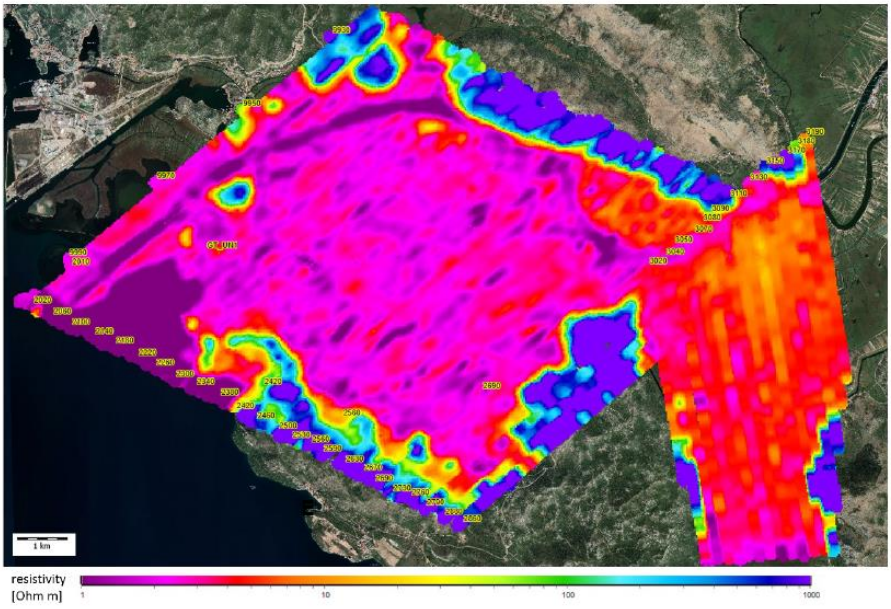

Figure 6.3 Resistivity slice at 10 m a.s.l.

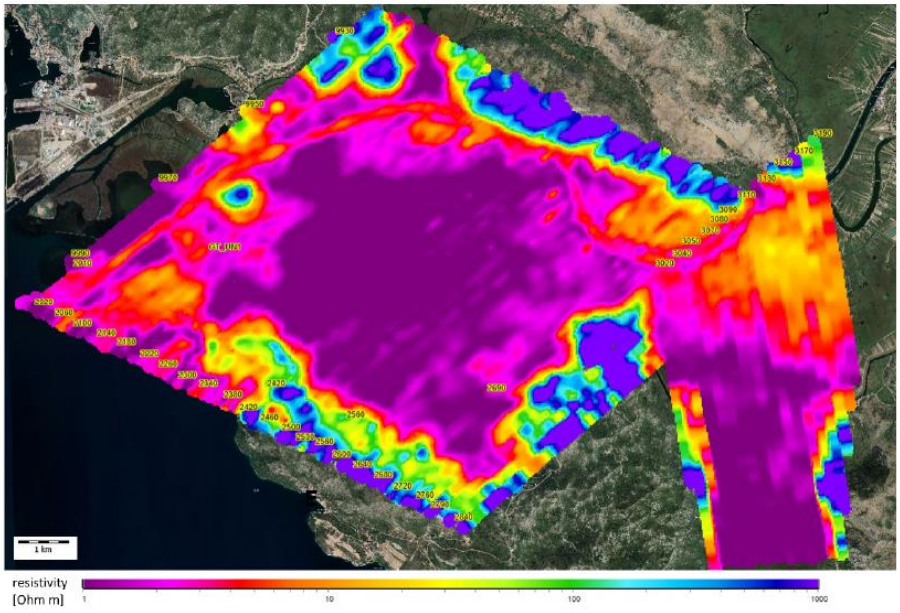

Figure 6.4 Resistivity slice at 25 m a.s.l.

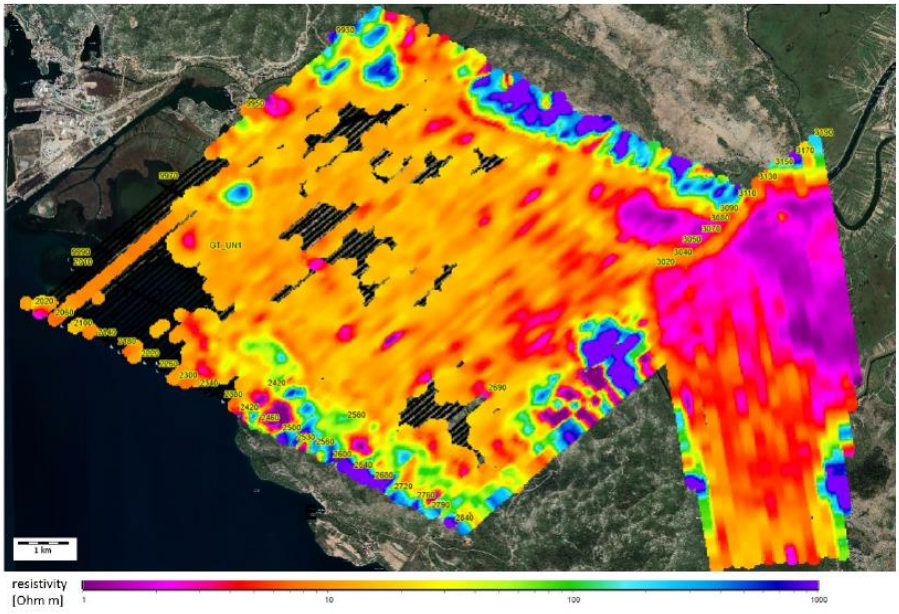

Figure 6.5 Resistivity slice at 50 m a.s.l.

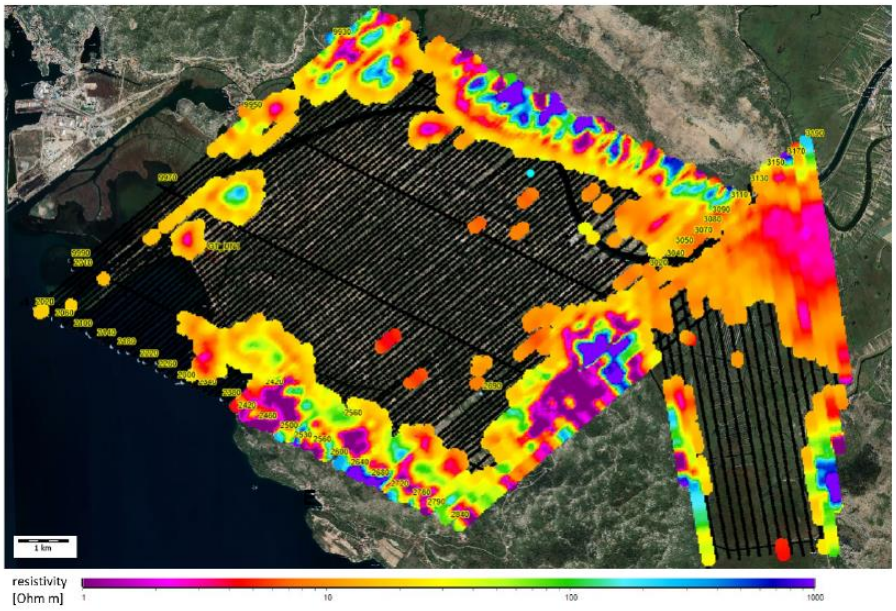

Figure 6.6 Resistivity slice at 70 m a.s.l

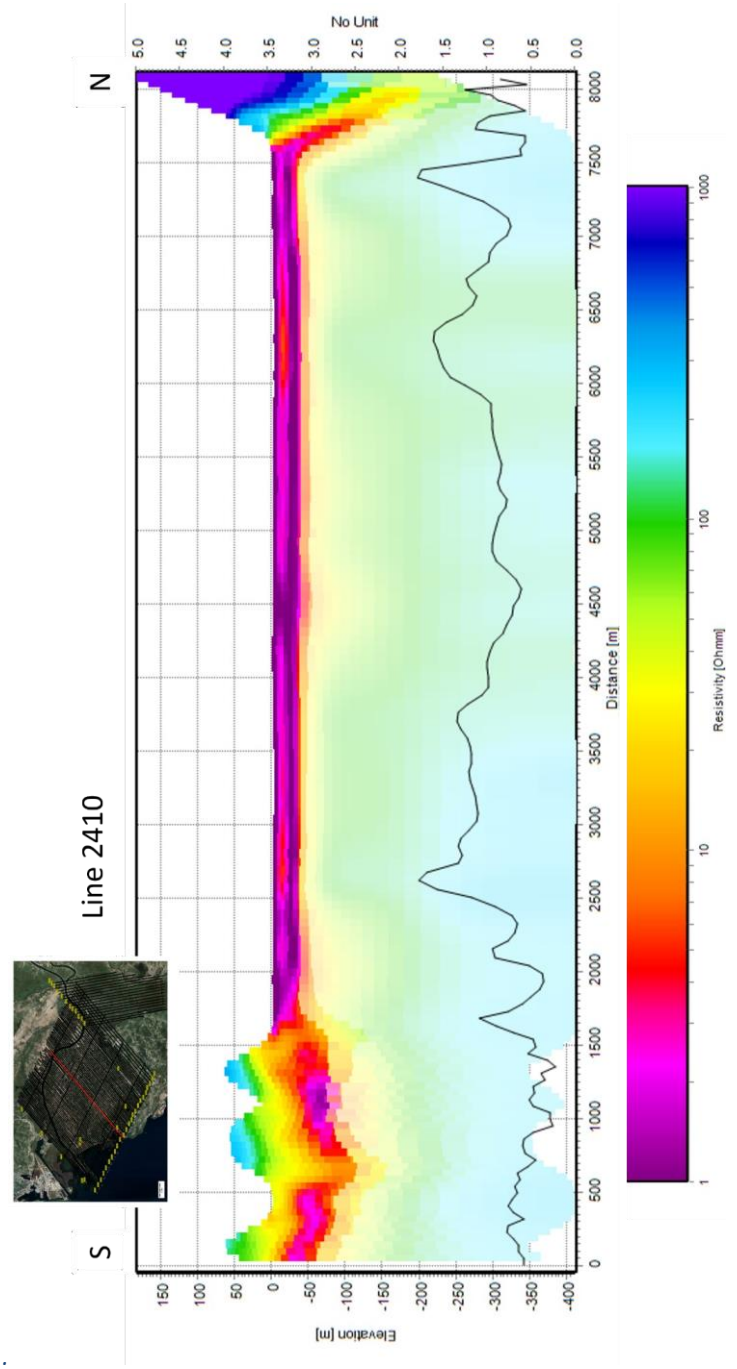

Figure 6.7 Resistivity vertical section along Flight Line 2410

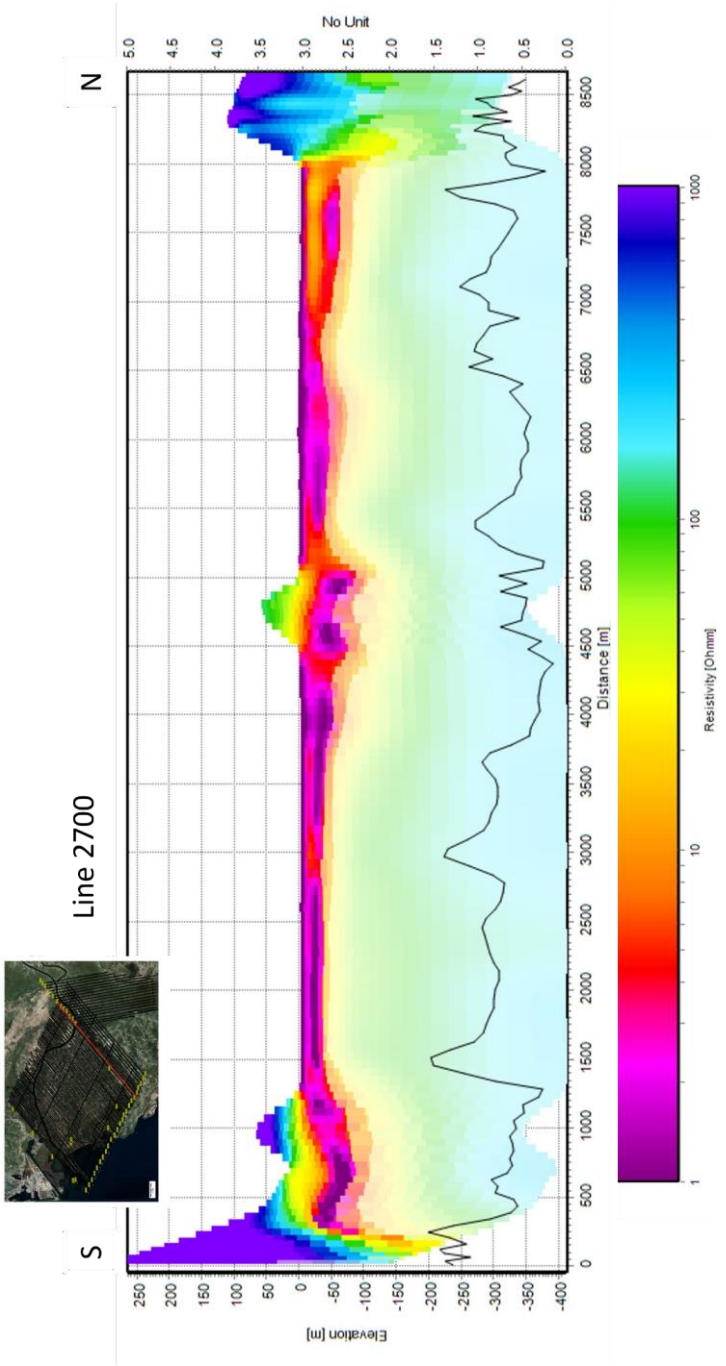

Figure 6.8 Resistivity vertical section along Flight Line 2700

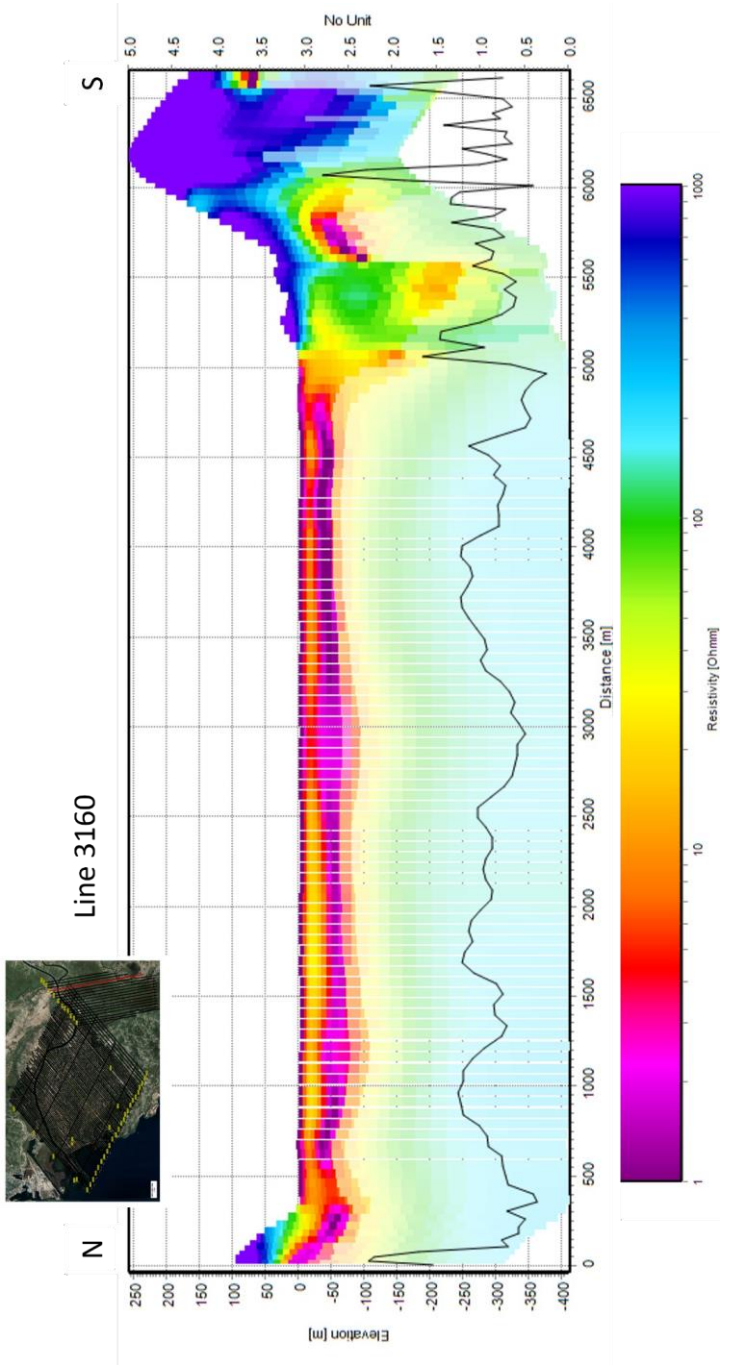

Figure 6.9 Resistivity vertical section along Flight Line 3160

7 Conclusions

The advanced processing carried out on the EQUATOR dataset is capable to provide very useful information for further geological-hydrogeological modeling.

In particular, already from the data (see, for example, Figure 4.3) and even more from the inversionresults, it is clear that the geology cannot be assumed horizontally layered: there are elongated resistive anomalies (crossing the flight lines – so, definitely, not due to possible "flight-line artifacts") that might be old meanders. For generating reliable hydrological scenarios, those features must be taken into account as potential preferential paths. In turn, considering a mere "layered cake" hydrostratigraphic model could lead to misleading conclusions.

Despite these promising preliminary results, further investigation of the data might lead to a more comprehensive and reliable picture of the survey volume. In particular, the three partners of the project are still actively working on the integration of the results from the frequency and time representations. In addition, the airborne data and the ground-based measurements that have been recently collected can be mutually beneficial and their joint inversion/interpretation can contribute to resolving inherent ambiguities of the geophysical methods.

8 Literature

Auken, E., A. V. Christiansen, J. A. Westergaard, C. Kirkegaard, N. Foged, and A. Viezzoli, (2009), An integrated processing scheme for high-resolution airborne electromagnetic surveys, the SkyTEM system, Exploration Geophysics, 40, 184-192

Christiansen, A. V., and E. Auken, (2012), A global measure for depth of investigation, Geophysics, 77, 4, WB171-WB177.

Viezzoli, A., A. V. Christiansen, E. Auken, and K. I. Sørensen, (2008), Quasi-3D modeling of airborne TEM data by Spatially Constrained Inversion, Geophysics, 73, 3, F105-F113.

Vignoli, G., G. Fiandaca, A.V. Christiansen, C. Kirkegaard, and E. Auken, (2015), Sharp spatially constrained inversion with applications to transient electromagnetic data, Geophysical Prospecting, 63, 243-255.

Vignoli, G., J. Guillemoteau, J. Barreto, and M. Rossi, (2021), Reconstruction, with tunable sparsity levels, of shear wave velocity profiles from surface wave data, Geophysical Journal International, 225(3), 1935-1951.

9 List of figures

10 List of tables